NANO LETTERS

pubs.acs.org/NanoLett Letter

Modeling Auger Processes with Nonadiabatic Molecular Dynamics

Guoqing Zhou, Gang Lu, and Oleg V. Prezhdo*

Cite This: *Nano Lett.* 2021, 21, 756–761 Read Online

ACCESS | Metrics & More | Article Recommendations | Supporting Information

ABSTRACT: Auger-type energy exchange plays key roles in the carrier dynamics in nanomaterials due to strong carrier−carrier interactions. However, theoretical descriptions are limited to perturbative calculations of scattering rates on static structures. We develop an accurate and efficient ab initio technique to model Auger scattering with nonadiabatic molecular dynamics. We incorporate the many-body Coulomb matrix into several surface hopping methods and describe simultaneously charge−charge and charge−phonon scattering in the time-domain and in a nonperturbative, configuration-dependent manner. The approach is illustrated with a CdSe quantum dot. Auger scattering between electrons and holes breaks the phonon bottleneck to electron relaxation. The bottleneck is recovered when electrons and holes are decoupled. The simulations correctly reproduce all experimental processes and time scales, including Auger- and phonon-assisted cooling of hot electrons, intraband carrier relaxation, and carrier recombination. Providing detailed insights into the energy flow, the developed method allows studies of carrier dynamics in nanomaterials with strong carrier−carrier interactions.

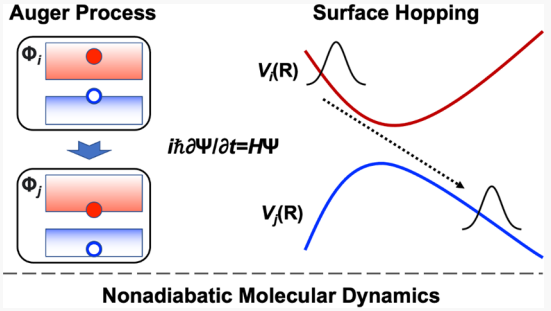

KEYWORDS: *Auger Process, Time-Dependent Density Functional Theory, Nonadiabatic Molecular Dynamics, Electron−Electron Scattering*

Nanomaterial exhibit extraordinary thermal, mechanical, and electronic properties and find wide applications in chemistry, engineering, and materials science. Carrier confinement is among the key factors underlying the great performance of nanomaterials. It is achieved by reduction of dimensionality, as in quantum dots (QDs) and wires and various layered systems, or by the creation of superlattice structures. Finding applications in optoelectronics, quantum confinement reduces electron−phonon scattering and enhances charge carrier lifetimes. At the same time, strong confinement augments carrier−carrier scattering, amplifies dissipative Auger-type processes, and shortens carrier lifetimes.[1−7]

In an Auger process, one electron falls from a high energy level into a lower level, and the released energy excites another carrier, possibly leading to its emission. Auger processes depend on carrier−carrier interactions and can break the "phonon bottleneck", arising in nanomaterials due to reduced electron−phonon scattering.[8−10] Auger-mediated carrier losses can accelerate carrier trapping and recombination, undermining electronic properties of nanomaterials. Various methods have been developed to inhibit Auger processes in nanosystems, such as separation of electrons and holes through doping and introduction of traps[10−12] or modification of nanostructure size and shape to reduce Auger efficiency.[3] There are few theoretical works on modeling quantum dynamics of Auger processes, because of the computational expense of electron−electron interactions.

Most theoretical works compute Auger transition rates with Fermi's golden rule based on electron−electron interactions from static configurations. Such a perturbative approach is computationally efficient, given the dense manifold of states and a tremendous number of Coulomb matrix elements.[3,4,13−17] Nevertheless, Coulomb interactions can be strong under quantum confinement, challenging the perturbation theory assumption of weak coupling. Further, a rate calculation assumes a particular kinetics, typically exponential, while quantum dynamics starts as a Gaussian and may develop complex time-dependence, especially with multiple competing processes, such as charge−charge and charge−phonon scattering, charge and energy transfer, polaron and exciton formation, spin transitions, etc., that can occur on similar time scales.[7,17,18] Moreover, charge distributions and Coulomb interactions can exhibit a strong dependence on atomic configuration, both in inorganic semiconductors[19] and especially in soft materials, such as metal halide perovskites[20,21] and organic matter.[22]

Two approaches have been used to model Auger-type quantum dynamics at the atomistic level of description and in

Received: November 9, 2020
Revised: December 9, 2020
Published: December 15, 2020

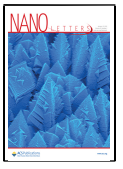

https://dx.doi.org/10.1021/acs.nanolett.0c04442
Nano Lett. 2021, 21, 756–761

the time-domain. One technique added intermediate high-energy states and decomposed a two-particle Auger transition into two single-particle transitions, as introduced by Kim et al.[17,23] Zhu et al. used this method to demonstrate Auger-assisted electron transfer between semiconductor quantum dots (QDs) and molecular acceptors using nonadiabatic (NA) molecular dynamics (MD).[24] Wang et al.[25] introduced the global flux surface hopping (GFSH) method to allow NA transitions involving multiple particles simultaneously. Still, both methods rely on single-particle coupling matrix elements and require many intermediate states in the calculation. The approaches have been used to model several systems and proved capable of reproducing experimental time scales.[7,12,26,27] Even though single-particle models have experienced huge successes, the physics of Auger processes resides in carrier−carrier interactions, and therefore, it is desirable to include such interactions into NAMD simulations explicitly.

In this Letter, we introduce the electron−electron interaction into NAMD, as implemented with ab initio real-time time-dependent DFT (TDDFT) in the PYXAID code.[28,29] We compute the many-body Coulomb matrix elements and incorporate them into the TDDFT equations-of-motion and surface hopping (SH) transition probabilities. These matrix elements are readily available in linear response TDDFT codes. In contrast to linear response TDDFT, we avoid diagonalization of large matrices, keeping the computational cost low. By incorporating both NA and Coulomb coupling, the methods allow for simultaneous modeling of the quantum dynamic of electron−phonon and electron−electron scattering in a nonperturbative, configuration-dependent way and in the time-domain. We test the developed method on a CdSe quantum dot (QD), which has been studied for light harvesting and optoelectronics both experimentally and theoretically and which constitutes a classic example of an Auger-type process in a nanomaterial.[1,3,11,12,30,31] With the spatial confinement, QDs are expected to have slow electronic transitions due to the mismatch between electronic and vibrational energy quanta. However, most QDs exhibit rapid bulklike relaxation. Our results show a sub-picosecond Auger process that outcompetes phonon-driven relaxation, in excellent agreement with experiments. Accurate and efficient, the developed method can be applied to various low-dimensional materials, in which charge−charge scattering provides an important pathway of energy flow.

The evolution of the multielectron wave function $\mathbf{\Psi}(\mathbf{r}, \mathbf{R}, t)$ is determined by the time-dependent Schrödinger equation (TDSE):

$$i\hbar\frac{\partial \mathbf{\Psi}(\mathbf{r}, \mathbf{R}, t)}{\partial t} = \boldsymbol{H}(\mathbf{r}, \mathbf{R}, t)\, \mathbf{\Psi}(\mathbf{r}, \mathbf{R}, t) \tag{1}$$

The Hamiltonian $\boldsymbol{H}$ of the electron-nuclei system depends explicitly on electronic coordinates $\mathbf{r}$, and parametrically on the nuclear coordinates R. $\mathbf{\Psi}(\mathbf{r}, \mathbf{R}, t)$ can be represented with a linear combination of basis functions $\Phi_i(\mathbf{r}|R)$:

$$\Psi(\mathbf{r}, \mathbf{R}, t) = \sum_i c_i(t)\, \Phi_i(\mathbf{r}|\mathbf{R}) \tag{2}$$

In the time-dependent Kohn−Sham (TDKS) theory,[28,29,32] the multielectron wave functions $\Phi_i(\mathbf{r}|R)$ are Slater determinants of adiabatic Kohn−Sham[33] (KS) orbitals φ_k that are computed with standard DFT packages. The TDSE is rewritten as

$$i\hbar\frac{\partial}{\partial t}c_i(t) = \sum_j (\varepsilon_i\delta_{ij} + d_{ij})c_j(t) \tag{3}$$

where δ_{ij} is the Kronecker delta, ε_i is the eigen-energy for basis function Φ_i, and d_{ij} is nonadiabatic coupling (NAC) between basis states Φ_i and Φ_j:

$$d_{ij} = -i\hbar\left\langle \Phi_i \middle| \frac{\partial}{\partial t} \middle| \Phi_j \right\rangle = -i\hbar\langle\Phi_i|\nabla_{\mathbf{R}}|\Phi_j\rangle\dot{\mathbf{R}} \tag{4}$$

Because d_{ij} is a one-electron operator, it is nonzero only if Slater determinants Φ_i and Φ_j differ by one KS orbital. The many-electron d_{ij} can be reduced to NAC between single-particle KS orbitals [see the Supporting Information (SI)].[28]

In order to incorporate explicitly carrier−carrier interactions into the NAMD simulations, we introduce the corresponding many-body terms into Hamiltonian $\mathbf{H}(\mathbf{r}, \mathbf{R}, t)$. The electron−electron interaction between states $\Phi_i = \Phi_m^n = |\varphi_1\, \varphi_m ... \varphi_n ... \varphi_N\rangle$ and $\Phi_j = \Phi_p^q = |\varphi_1\, \varphi_p ... \varphi_q ... \varphi_N\rangle$ is evaluated as

$$V_{ij} = \langle\Phi_m^n|\hat{V}|\Phi_p^q\rangle = \langle mn|pq\rangle - \langle mn|qp\rangle \tag{5}$$

Here, $\langle mn|pq\rangle$ is the Coulomb integral:

$$\langle mn|pq\rangle = \frac{e^2}{2}\int \mathrm{d}\mathbf{r}_1\, \mathrm{d}\mathbf{r}_2 \varphi_m^*(\mathbf{r}_1)\, \varphi_n^*(\mathbf{r}_2) r_{12}^{-1} \varphi_p(\mathbf{r}_1)\, \varphi_q(\mathbf{r}_2) \tag{6}$$

The Coulomb tetradic tensor in eq 6 is evaluated with the projector augmented wave (PAW) methodology (see the SI).[34,35] The single-particle tensor gives the interaction matrix for many-particle Slater determinants Φ_i (see eq 5). The matrix elements in eq 5 are nonzero for multiparticle states that differ in two electronic orbitals, and therefore, they describe electron−electron scattering. The two-particle interaction describes energy flows from electrons to holes considered in the example below. It also describes Auger-assisted charge trapping, in which a particle being trapped gives excess energy to another particle, and Auger-assisted electron−hole recombination, in which an electron hopping from the conduction to valence band edge gives energy to another electron. Higher-order processes, such as annihilation of a double exciton into a single exciton, can be introduced using Coulomb interactions arising in the Bethe−Salpeter theory.[36] Dielectric screening of Coulomb interactions can be included using a material's dielectric constant or, more rigorously, the frequency-dependent dielectric matrix of the GW theory.[37,38]

With the addition of the Coulomb matrix elements, the Hamiltonian H_{ij} in eq 3 is updated to

$$H_{ij} = \varepsilon_i\delta_{ij} + d_{ij} + V_{ij} \tag{7}$$

The NAC d_{ij}, eq 4, describes electron-vibrational interactions, while the Coulomb matrix element V_{ij}, eq 5, generates electron−electron scattering. Thus, both types of interactions are included in the TDSE.

Hamiltonians of this type, eq 7, but without d_{ij}, are commonly used in linear response TDDFT and many-body wave function models.[36,39−43] Excited state energies are obtained as eigen-energies of the many-body Hamiltonian, and the wave functions are expressed as superpositions of many Slater determinants. The large dimensionality of many-body Hamiltonians limits the solution of the eigenvalue problem to small systems and few excited states. Our approach does not require finding eigenstates of the many-body Hamiltonian. Instead, the Hamiltonian, eq 7, is used to propagate the TDSE in the Slater determinant basis. Even if

https://dx.doi.org/10.1021/acs.nanolett.0c04442
Nano Lett. 2021, 21, 756−761

diagonalization of the many-body Hamiltonian is feasible, it is easier to interpret simulations in the Slater determinant basis, since Auger-type energy exchange between charge carriers assumes the single-particle picture. Simulations in the adiabatic many-body representation are more suitable for studying processes involving bound electron−hole pairs, i.e., excitons.

The Hamiltonian, eq 7, can be used in any SH technique. We have implement the method within Tully's fewest switches SH (FSSH)[44] that is the most popular SH approach, the GFSH[25] generalization of FSSH, and decoherence-induced SH (DISH).[45] The transition probability for Tully's FSSH is given by

$$P_{i\to j}(t,\,\mathrm{d}t) = \int_{t}^{t+\mathrm{d}t} \frac{2}{\|c_i(t)^2\|} Re\left[\left(\frac{i(d_{ij}+V_{ij})}{\hbar}\right) c_i^*(t)\, c_j(t)\right] \mathrm{d}t \tag{8}$$

where d_{ij} and V_{ij} are the NAC and Coulomb matrix elements, eqs 4 and 5, and the coefficients $c_i(t)$ are solutions of the TDSE, eq 1, in the Slater determinant basis, eq 2. FSSH only allows transitions between states that are directly coupled, as its probability is proportional to the coupling strength, eq 8. As such, FSSH does not allow for the superexchange mechanism, in which two states are not coupled directly, but through a third state. To account for this deficiency, FSSH was generalized in GFSH that allows transitions between states that are not coupled directly.[25] The DISH approach is another recent SH scheme that does not have this deficiency.[45] Compared to FSSH and many other SH techniques that employ different ad hoc expressions for state-to-state transition rates, the transition probabilities in DISH are given by the quantum mechanical probabilities, i.e., squares of the $c_i(t)$ coefficients, directly. Further, DISH is rooted in the theory of quantum open systems[46,47] and naturally incorporates decoherence effects. The simulations reported below are performed with the DISH approach.

The approach is implemented within the PYXAID software package.[28,29] Because KS orbitals φ_k obtained from standard DFT packages are specified up to an arbitrary phase that can change between MD time steps, we enforce phase-consistency.[48] In order to eliminate trivial crossings,[49] we keep track of orbital ordering.[50] The simulations are performed with VASP using the Perdew−Burke−Ernzerhof (PBE) exchange-correlation functional and the PAW method.[51−56] The NAC are computed using the methodology developed recently for the PAW method[57] based on the Pawpyseed package.[58]

We illustrate the method by investigating electron cooling in the $Cd_{33}Se_{33}$ QD, Figure 1a, since it constitutes a classic example in which Auger-type energy exchange between electrons and holes breaks the bottleneck to the phonon-mediated relaxation.[1] Simulation details are provided in the SI. The QD diameter is 1.4 nm. The electronic density of states (DOS), computed for the optimized geometry, exhibits an isolated state at the conduction band (CB) edge (see Figure 1b). The state, commonly denoted as $1S_e$, corresponds to the lowest unoccupied molecular orbital (LUMO) and couples weakly to other states. Figure 1c demonstrates phonon-driven evolution of the energies of the highest occupied molecular orbital (HOMO) and the $1S_e$ and $1P_e$ (LUMO+1) states along the MD trajectory. The $1S_e$ state remains separated from the CB at room temperature as well. The large gap (0.43 eV) between $1S_e$ and $1P_e$ prohibits rapid nonradiative relaxation of

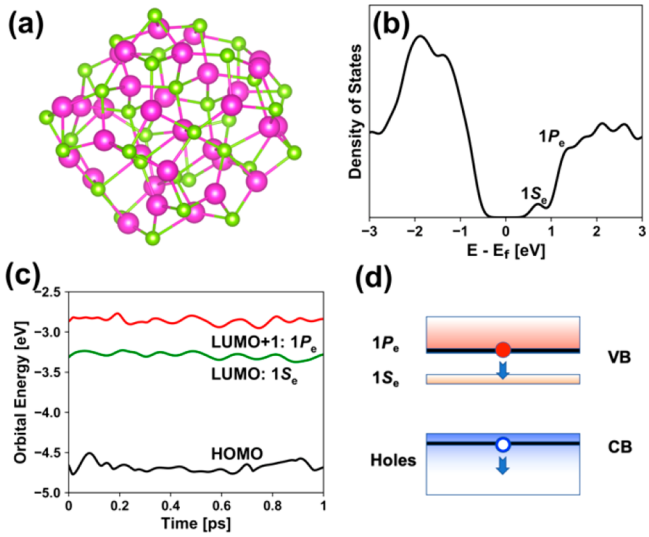

Figure 1. (a) Optimized structure of the $Cd_{33}Se_{33}$ QD (Cd, magenta; Se, green). (b) Electronic density of states for the QD. The DOS is higher in the valence band than in the conduction band. The LUMO ($1S_e$) is isolated from the LUMO+1 ($1P_e$) and the rest of the band. (c) Phonon-induced fluctuations of the orbital energies along the MD trajectory. (d) Schematic of the Auger-type process, in which the hot electron cools from $1P_e$ to $1S_e$ while exciting the hole to deeper levels.

hot electrons; i.e., there exists a phonon bottleneck.[9,10] The bottleneck can only be observed experimentally, if the valence band (VB) hole is decoupled from the electron.[10] If both electron and hole are present in the QD and can exchange energy, the bottleneck is broken.[1,12]

A hot electron deep inside the CB relaxes rapidly through the dense manifold of states to $1P_e$ by coupling to phonons. Then, the electron hops from $1P_e$ to $1S_e$ via the Auger process, depositing its energy to the hole that is excited from the VB edge deeper into the band (see Figure 1d). The hole relaxes rapidly to the VB edge through phonons. Finally, the electron and hole recombine across the band gap, depositing the excess energy to vibrations. In the presence of more charge carriers, e.g., the trion[59] or double exciton,[16] the energy released during the recombination can be deposited into the extra carriers. These types of Auger processes are not presently considered.

Figure 2a,b demonstrates the sub-picosecond Auger process occurring due to the Coulomb interaction. Both multielectron and single-electron state populations are shown. The simulation is started with the excitation Φ_H^{L1}: HOMO → $1P_e$. State Φ_H^{L1} decays quickly, within ∼0.2 ps, and at the same time, the group of states Φ_{DHs}^{L} (HOMO−1 and below → LUMO) gets populated (see Figure 2a). At the single-particle level, Figure 2b, the hot electron jumps from $1P_e$ into $1S_e$ within 0.2 ps. At the same time, the hole residing initially in the HOMO gets excited into deep hole levels (DHs). Subsequently, the deep hole relaxes quickly, on a sub-picosecond time scale, back to the HOMO, as seen in the bell-shape curves in Figure 2a for Φ_{DHs}^{L} and Figure 2b for DHs, and the inverse, V-shape curve for the HOMO. The Auger process followed by the quick hole relaxation bypasses the phonon bottleneck.

In comparison, the simulation without the many-body electron interaction misses the Auger process. In Figure 2c, the population of the states Φ_{Hs}^{L1} (HOMO and below → LUMO+1) decays slightly after 40 ps, and the hole excited states Φ_{Hs}^{L} (HOMO and below → LUMO) are not involved at

https://dx.doi.org/10.1021/acs.nanolett.0c04442
Nano Lett. 2021, 21, 756−761

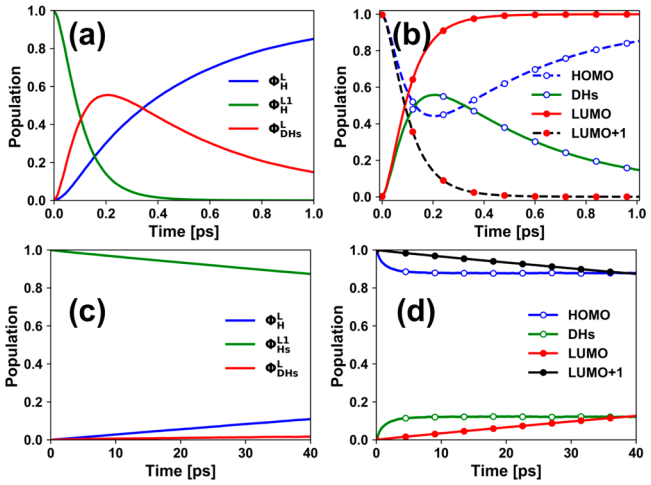

Figure 2. State populations illustrating the Auger process. (a, c) Populations of the multielectron states during NAMD with and without Coulomb scattering, respectively. Φ_H^L represents the HOMO → LUMO excitation (blue). Φ_{Hs}^{L1} represents all excitations from HOMO and below to LUMO+1, green. Φ_{DHs}^{L} represents all excitations from HOMO−1 and below to LUMO (red). (b, d) Corresponding single-particle populations during NAMD with and without Coulomb scattering, respectively. DHs (deep holes) represent all holes in HOMO−1 and lower states.

all. In Figure 2d, the population of the hot electron, initially residing in $1P_e$, decays only slightly after 40 ps. The hole rapidly equilibrates among levels within k_BT around the HOMO due to the strong NAC between these states. The DHs never get significantly populated (cf. Figure 2b). Without the Coulomb interaction, the electron decays from $1P_e$ to $1S_e$ within hundreds of picoseconds, as observed in the experiments with holes decoupled from electrons.[10] Therefore, the many-body electron interaction is essential for modeling the Auger process.

Table 1 summarizes time scales of the various processes. Additional results and discussion are provided in the SI.

Table 1. Time Scales for Hot Electron Relaxation to LUMO +1, Hot Hole Relaxation to HOMO, LUMO+1 → LUMO ($1P_e \rightarrow 1S_e$) Transition, and Charge Recombination[a]

	with Coulomb V_{ij}	without Coulomb
electron relaxing to LUMO+1		0.3 ps
hole relaxing to HOMO		0.2−0.3 ps
LUMO+1 → LUMO	0.15 ps	210 ps
electron−hole recombination	1000 ps	1000 ps

[a]The hot electron/hole relaxations were modeled as single-particle processes, not allowing energy exchange between particles. Simulations of the $1P_e \rightarrow 1S_e$ transition and electron−hole recombination included both the electron and hole.

Comparisons of the NAC and Coulomb matrix elements are provided in Figure S1 and Table S1. The NAC for adjacent states is around 20 meV in the VB and 10 meV in the CB, rationalizing the fast intraband relaxation. The NACs across the gaps between $1P_e$−$1S_e$, and $1S_e$−ground state are 1 to 2 orders of magnitude smaller. The Coulomb matrix elements are around 10−40 meV between states Φ_H^{L1} (HOMO → LUMO+1) and Φ_{Hp}^{L} (HOMO−14, ..., HOMO → LUMO, p = 0, ..., 0.14), rationalizing why the Auger scattering is fast and breaks the phonon bottleneck. As shown by Rabani and coworkers,[16,60] the Coulomb matrix elements decrease significantly with increasing QD size. The electron−phonon interaction decreases with system size at a slower pace, such that the two interactions are comparable for QDs used in most experiments. In bulk, the Coulomb interaction is weaker than the electron−phonon interaction. The energy flow between the electronic and vibrational subsystems is analyzed in Figures S2−S5, and frequencies of active phonon modes are identified. Electrons and holes relax within dense band manifolds on 0.15−0.4 ps time scales depending on the initial energy. After the electron relaxes to $1P_e$, it exchanges energy with the hole on a 0.15 ps time scale and drops to $1S_e$. Then, the hole rapidly relaxes to the band edge. In the absence of other charges, the electron−hole recombination takes 1 ns.

In summary, we have developed and demonstrated an efficient technique for modeling Auger-type processes with NAMD. The quantum dynamics calculation incorporates simultaneously electron−phonon and electron−electron scattering processes in a nonperturbative manner with explicit dependence on atomic configuration. In addition to the NAC that describes electron-vibrational interactions, we have incorporated the Coulomb coupling that captures many-body electron interactions. In particular, the Coulomb matrix elements can couple states that differ by two KS orbitals and, therefore, allow transitions in which two particles exchange energy. The methodology has been implemented within several SH schemes. The additional expense of the calculation arises from the need to obtain configuration-dependent Coulomb matrix elements, which are computed routinely in linear response TDDFT. In contrast to linear response TDDFT, the current method does not require diagonalization of large matrices, and the additional expense is minimal.

The developed technique has been demonstrated by application to the Auger-assisted relaxation of hot electrons in a CdSe QD. This problem constitutes a classic example of an Auger process in a nanoscale material. The Auger-type energy exchange between electron and hole breaks the phonon bottleneck to the hot electron relaxation. The bottleneck can be recovered only when the hole is decoupled from the electron. Our simulations demonstrate all processes observed experimentally and reproduce the experimental time scales. Importantly, Auger-type and phonon-assisted processes can occur in parallel on similar time scales and compete with each other. Therefore, it is necessary to model them simultaneously, as achieved by the developed technique. The method makes no perturbative assumptions, as is often the case in rate calculations. This is important, because Coulomb interactions can be strong in confined systems. Further, the quantum dynamics simulations enabled by the developed approach differ from kinetics calculations that have to assume a particular kinetic mechanism, e.g., first or second order, Gaussian or exponential. The NAC and Coulomb terms depend explicitly on the nuclear configuration, which is particularly important for studying softer materials, such as metal halide perovskites and organic matter, as well as in organic materials with surfaces, edges, and defects, since such systems can undergo large-scale anharmonic motions as a result of both finite temperature and electronic excitation.[61,62] The direct modeling of Auger processes with NAMD captures realistic aspects of the materials' atomic structure and provides an efficient and accurate approach for studying carrier dynamics in low-dimensional materials.

https://dx.doi.org/10.1021/acs.nanolett.0c04442
Nano Lett. 2021, 21, 756−761

■ ASSOCIATED CONTENT

Supporting Information

The Supporting Information is available free of charge at https://pubs.acs.org/doi/10.1021/acs.nanolett.0c04442.

Details of computation of the Coulomb and nonadiabatic coupling matrix elements, comment on time-dependent Kohn−Sham equations and nonadiabatic molecular dynamics, simulation details, and analysis of energy flow between electronic and vibrational subsystems (PDF)

■ AUTHOR INFORMATION

Corresponding Author

Oleg V. Prezhdo − *Department of Physics and Astronomy and Department of Chemistry, University of Southern California, Los Angeles, California 90089, United States;* orcid.org/0000-0002-5140-7500; Email: prezhdo@usc.edu

Authors

Guoqing Zhou − *Department of Physics and Astronomy, University of Southern California, Los Angeles, California 90089, United States;* orcid.org/0000-0002-4000-8467

Gang Lu − *Department of Physics and Astronomy, California State University, Northridge, California 91330, United States;* orcid.org/0000-0002-9168-8968

Complete contact information is available at: https://pubs.acs.org/10.1021/acs.nanolett.0c04442

Notes

The authors declare no competing financial interest.

■ ACKNOWLEDGMENTS

G.Z. and O.V.P. acknowledge funding of the U.S. National Science Foundation, grant CHE-1900510. G.L. acknowledges the support of the Army Research Office (W911NF1810473).

■ REFERENCES

(1) Efros, A. L.; Kharchenko, V. A.; Rosen, M. Breaking the Phonon Bottleneck in Nanometer Quantum Dots - Role of Auger-Like Processes. *Solid State Commun.* **1995**, *93*, 281−284.

(2) Klimov, V. I.; Mikhailovsky, A. A.; McBranch, D. W.; Leatherdale, C. A.; Bawendi, M. G. Quantization of Multiparticle Auger Rates in Semiconductor Quantum Dots. *Science* **2000**, *287*, 1011−1013.

(3) Cragg, G. E.; Efros, A. L. Suppression of Auger Processes in Confined Structures. *Nano Lett.* **2010**, *10*, 313−317.

(4) Philbin, J. P.; Rabani, E. Electron-Hole Correlations Govern Auger Recombination in Nanostructures. *Nano Lett.* **2018**, *18*, 7889−7895.

(5) Covito, F.; Perfetto, E.; Rubio, A.; Stefanucci, G. Real-Time Dynamics of Auger Wave Packets and Decays in Ultrafast Charge Migration Processes. *Phys. Rev. A: At., Mol., Opt. Phys.* **2018**, *97*, 061401.

(6) Gao, J. B.; Kidon, L.; Rabani, E.; Alivisatos, A. P. Ultrahigh Hot Carrier Transient Photocurrent in Nanocrystal Arrays by Auger Recombination. *Nano Lett.* **2019**, *19*, 4804−4810.

(7) Li, L. Q.; Lin, M. F.; Zhang, X.; Britz, A.; Krishnamoorthy, A.; Ma, R. R.; Kalia, R. K.; Nakano, A.; Vashishta, P.; Ajayan, P.; et al. Phonon-Suppressed Auger Scattering of Charge Carriers in Defective Two-Dimensional Transition Metal Dichalcogenides. *Nano Lett.* **2019**, *19*, 6078−6086.

(8) Nozik, A. J.; Beard, M. C.; Luther, J. M.; Law, M.; Ellingson, R. J.; Johnson, J. C. Semiconductor Quantum Dots and Quantum Dot Arrays and Applications of Multiple Exciton Generation to Third-Generation Photovoltaic Solar Cells. *Chem. Rev.* **2010**, *110*, 6873−6890.

(9) Kilina, S. V.; Neukirch, A. J.; Habenicht, B. F.; Kilin, D. S.; Prezhdo, O. V. Quantum Zeno Effect Rationalizes the Phonon Bottleneck in Semiconductor Quantum Dots. *Phys. Rev. Lett.* **2013**, *110*, 180404.

(10) Pandey, A.; Guyot-Sionnest, P. Slow Electron Cooling in Colloidal Quantum Dots. *Science* **2008**, *322*, 929−932.

(11) Wang, L.; Chen, Z.; Liang, G.; Li, Y.; Lai, R.; Ding, T.; Wu, K. Observation of a Phonon Bottleneck in Copper-Doped Colloidal Quantum Dots. *Nat. Commun.* **2019**, *10*, 1−8.

(12) Trivedi, D. J.; Wang, L.; Prezhdo, O. V. Auger-Mediated Electron Relaxation Is Robust to Deep Hole Traps: Time-Domain Ab Initio Study of Cdse Quantum Dots. *Nano Lett.* **2015**, *15*, 2086−2091.

(13) Mocker, M.; Lemke, F. Theoretical Results on the Efficiency of Auger Recombination in Low Dimensional Pbsnte Structures. *Superlattices Microstruct.* **1991**, *10*, 231−234.

(14) Landau, L. D.; Lifshitz, E. M. *Quantum Mechanics: Non-Relativistic Theory*; Pergamon Press: Oxford, 1991.

(15) Danilov, L.; Zegrya, G. Theoretical Study of Auger Recombination Processes in Deep Quantum Wells. *Semiconductors* **2008**, *42*, 550−556.

(16) Philbin, J. P.; Rabani, E. Auger Recombination Lifetime Scaling for Type I and Quasi-Type Ii Core/Shell Quantum Dots. *J. Phys. Chem. Lett.* **2020**, *11*, 5132−5138.

(17) Hyeon-Deuk, K.; Prezhdo, O. V. Time-Domain Ab Initio Study of Auger and Phonon-Assisted Auger Processes in a Semiconductor Quantum Dot. *Nano Lett.* **2011**, *11*, 1845−1850.

(18) Ben-Shahar, Y.; Philbin, J. P.; Scotognella, F.; Ganzer, L.; Cerullo, G.; Rabani, E.; Banin, U. Charge Carrier Dynamics in Photocatalytic Hybrid Semiconductor-Metal Nanorods: Crossover from Auger Recombination to Charge Transfer. *Nano Lett.* **2018**, *18*, 5211−5216.

(19) Balan, A. D.; Eshet, H.; Olshansky, J. H.; Lee, Y. V.; Rabani, E.; Alivisatos, A. P. Effect of Thermal Fluctuations on the Radiative Rate in Core/Shell Quantum Dots. *Nano Lett.* **2017**, *17*, 1629−1636.

(20) Zhou, G. Q.; Chu, W. B.; Prezhdo, O. V. Structural Deformation Controls Charge Losses in Mapbi(3): Unsupervised Machine Learning of Nonadiabatic Molecular Dynamics. *Acs Energy Letters* **2020**, *5*, 1930−1938.

(21) Zhang, Z. S.; Long, R.; Tokina, M. V.; Prezhdo, O. V. Interplay between Localized and Free Charge Carriers Can Explain Hot Fluorescence in the Ch3nh3pbbr3 Perovskite: Time-Domain Ab Initio Analysis. *J. Am. Chem. Soc.* **2017**, *139*, 17327−17333.

(22) Kilina, S.; Batista, E. R.; Yang, P.; Tretiak, S.; Saxena, A.; Martin, R. L.; Smith, D. L. Electronic Structure of Self-Assembled Amorphous Polyfluorenes. *ACS Nano* **2008**, *2*, 1381−1388.

(23) Hyeon-Deuk, K.; Prezhdo, O. V. Multiple Exciton Generation and Recombination Dynamics in Small Si and Cdse Quantum Dots: An Ab Initio Time-Domain Study. *ACS Nano* **2012**, *6*, 1239−1250.

(24) Zhu, H.; Yang, Y.; Hyeon-Deuk, K.; Califano, M.; Song, N.; Wang, Y.; Zhang, W.; Prezhdo, O. V.; Lian, T. Auger-Assisted Electron Transfer from Photoexcited Semiconductor Quantum Dots. *Nano Lett.* **2014**, *14*, 1263−1269.

(25) Wang, L.; Trivedi, D.; Prezhdo, O. V. Global Flux Surface Hopping Approach for Mixed Quantum-Classical Dynamics. *J. Chem. Theory Comput.* **2014**, *10*, 3598−3605.

(26) Dong, S.; Pal, S.; Lian, J.; Chan, Y.; Prezhdo, O. V.; Loh, Z.-H. Sub-Picosecond Auger-Mediated Hole-Trapping Dynamics in Colloidal Cdse/Cds Core/Shell Nanoplatelets. *ACS Nano* **2016**, *10*, 9370−9378.

(27) Pal, S.; Casanova, D.; Prezhdo, O. V. Effect of Aspect Ratio on Multiparticle Auger Recombination in Single-Walled Carbon Nanotubes: Time Domain Atomistic Simulation. *Nano Lett.* **2018**, *18*, 58−63.

(28) Akimov, A. V.; Prezhdo, O. V. The Pyxaid Program for Non-Adiabatic Molecular Dynamics in Condensed Matter Systems. *J. Chem. Theory Comput.* **2013**, *9*, 4959−4972.

(29) Akimov, A. V.; Prezhdo, O. V. Advanced Capabilities of the Pyxaid Program: Integration Schemes, Decoherenc:E Effects, Multi-excitonic States, and Field-Matter Interaction. *J. Chem. Theory Comput.* **2014**, *10*, 789−804.
(30) Cooney, R. R.; Sewall, S. L.; Anderson, K. E.; Dias, E. A.; Kambhampati, P. Breaking the Phonon Bottleneck for Holes in Semiconductor Quantum Dots. *Phys. Rev. Lett.* **2007**, *98*, 177403.
(31) Schaller, R. D.; Pietryga, J. M.; Goupalov, S. V.; Petruska, M. A.; Ivanov, S. A.; Klimov, V. I. Breaking the Phonon Bottleneck in Semiconductor Nanocrystals Via Multiphonon Emission Induced by Intrinsic Nonadiabatic Interactions. *Phys. Rev. Lett.* **2005**, *95*, 196401.
(32) Craig, C. F.; Duncan, W. R.; Prezhdo, O. V. Trajectory Surface Hopping in the Time-Dependent Kohn-Sham Approach for Electron-Nuclear Dynamics. *Phys. Rev. Lett.* **2005**, *95*, 163001.
(33) Kohn, W.; Sham, L. J. Self-Consistent Equations Including Exchange and Correlation Effects. *Phys. Rev.* **1965**, *140*, A1133.
(34) Zhang, X.; Lu, G. First-Order Nonadiabatic Couplings in Extended Systems by Time-Dependent Density Functional Theory. *J. Chem. Phys.* **2018**, *149*, 244103.
(35) Paier, J.; Hirschl, R.; Marsman, M.; Kresse, G. The Perdew-Burke-Ernzerhof Exchange-Correlation Functional Applied to the G2−1 Test Set Using a Plane-Wave Basis Set. *J. Chem. Phys.* **2005**, *122*, 234102.
(36) Wing, D.; Haber, J. B.; Noff, R.; Barker, B.; Egger, D. A.; Ramasubramaniam, A.; Louie, S. G.; Neaton, J. B.; Kronik, L. Comparing Time-Dependent Density Functional Theory with Many-Body Perturbation Theory for Semiconductors: Screened Range-Separated Hybrids and the Gw Plus Bethe-Salpeter Approach. *Physical Review Materials* **2019**, *3*, 064603.
(37) Shishkin, M.; Kresse, G. Implementation and Performance of the Frequency-Dependent G W Method within the Paw Framework. *Phys. Rev. B: Condens. Matter Mater. Phys.* **2006**, *74*, 035101.
(38) Shishkin, M.; Kresse, G. Self-Consistent G W Calculations for Semiconductors and Insulators. *Phys. Rev. B: Condens. Matter Mater. Phys.* **2007**, *75*, 235102.
(39) Krylov, A. I. Equation-of-Motion Coupled-Cluster Methods for Open-Shell and Electronically Excited Species: The Hitchhiker's Guide to Fock Space. *Annu. Rev. Phys. Chem.* **2008**, *59*, 433−462.
(40) Zhang, X.; Li, Z.; Lu, G. A Non-Self-Consistent Range-Separated Time-Dependent Density Functional Approach for Large-Scale Simulations. *J. Phys.: Condens. Matter* **2012**, *24*, 205801.
(41) Helbig, N.; Fuks, J. I.; Tokatly, I. V.; Appel, H.; Gross, E. K. U.; Rubio, A. Time-Dependent Density-Functional and Reduced Density-Matrix Methods for Few Electrons: Exact Versus Adiabatic Approximations. *Chem. Phys.* **2011**, *391*, 1−10.
(42) Castro, A.; Marques, M. A. L.; Alonso, J. A.; Rubio, A. Optical Properties of Nanostructures from Time-Dependent Density Functional Theory. *J. Comput. Theor. Nanosci.* **2004**, *1*, 231−255.
(43) Marques, M. A. L.; Gross, E. K. U. Time-Dependent Density Functional Theory. *Annu. Rev. Phys. Chem.* **2004**, *55*, 427−455.
(44) Tully, J. C. Molecular Dynamics with Electronic Transitions. *J. Chem. Phys.* **1990**, *93*, 1061−1071.
(45) Jaeger, H. M.; Fischer, S.; Prezhdo, O. V. Decoherence-Induced Surface Hopping. *J. Chem. Phys.* **2012**, *137*, 22A545.
(46) Gisin, N.; Percival, I. C. The Quantum-State Diffusion-Model Applied to Open Systems. *J. Phys. A: Math. Gen.* **1992**, *25*, 5677−5691.
(47) Prezhdo, O. V. Mean Field Approximation for the Stochastic Schrodinger Equation. *J. Chem. Phys.* **1999**, *111*, 8366−8377.
(48) Akimov, A. V. A Simple Phase Correction Makes a Big Difference in Nonadiabatic Molecular Dynamics. *J. Phys. Chem. Lett.* **2018**, *9*, 6096−6102.
(49) Wang, L. J.; Prezhdo, O. V. A Simple Solution to the Trivial Crossing Problem in Surface Hopping. *J. Phys. Chem. Lett.* **2014**, *5*, 713−719.
(50) Fernandez-Alberti, S.; Roitberg, A. E.; Nelson, T.; Tretiak, S. Identification of Unavoided Crossings in Nonadiabatic Photoexcited Dynamics Involving Multiple Electronic States in Polyatomic Conjugated Molecules. *J. Chem. Phys.* **2012**, *137*, 014512.
(51) Kresse, G.; Furthmuller, J. Efficient Iterative Schemes for Ab Initio Total-Energy Calculations Using a Plane-Wave Basis Set. *Phys. Rev. B: Condens. Matter Mater. Phys.* **1996**, *54*, 11169−11186.
(52) Kresse, G.; Furthmuller, J. Efficiency of Ab-Initio Total Energy Calculations for Metals and Semiconductors Using a Plane-Wave Basis Set. *Comput. Mater. Sci.* **1996**, *6*, 15−50.
(53) Kresse, G.; Hafner, J. Ab Initio Molecular-Dynamics Simulation of the Liquid-Metal-Amorphous-Semiconductor Transition in Germanium. *Phys. Rev. B: Condens. Matter Mater. Phys.* **1994**, *49*, 14251.
(54) Kresse, G. Ab-Initio Molecular-Dynamics for Liquid-Metals. *J. Non-Cryst. Solids* **1995**, *193*, 222−229.
(55) Perdew, J. P.; Burke, K.; Ernzerhof, M. Generalized Gradient Approximation Made Simple. *Phys. Rev. Lett.* **1996**, *77*, 3865−3868.
(56) Blochl, P. E. Projector Augmented-Wave Method. *Phys. Rev. B: Condens. Matter Mater. Phys.* **1994**, *50*, 17953−17979.
(57) Chu, W. B.; Zheng, Q.; Akimov, A. V.; Zhao, J.; Saidi, W.; Prezhdo, O. V. Accurate Computation of Nonadiabatic Coupling with Projector Augmented-Wave Pseudopotentials. *J. Phys. Chem. Lett.* **2020**, *11*, 10073−10080.
(58) Bystrom, K.; Broberg, D.; Dwaraknath, S.; Persson, K. A.; Asta, M. Pawpyseed: Perturbation-Extrapolation Band Shifting Corrections for Point Defect Calculations. *arXiv.org*, 2019, arXiv:1904.11572. https://kylebystrom.github.io/pawpyseed/ (accessed Dec, 31, 2019).
(59) Isborn, C. M.; Prezhdo, O. V. Charging Quenches Multiple Exciton Generation in Semiconductor Nanocrystals: First-Principles Calculations on Small Pbse Clusterse. *J. Phys. Chem. C* **2009**, *113*, 12617−12621.
(60) Rabani, E.; Baer, R. Distribution of Multiexciton Generation Rates in Cdse and Inas Nanocrystals. *Nano Lett.* **2008**, *8*, 4488−4492.
(61) Chu, W. B.; Saidi, W. A.; Prezhdo, O. V. Long-Lived Hot Electron in a Metallic Particle for Plasmonics and Catalysis: Ab Initio Nonadiabatic Molecular Dynamics with Machine Learning. *ACS Nano* **2020**, *14*, 10608−10615.
(62) Li, W.; Vasenko, A. S.; Tang, J. F.; Prezhdo, O. V. Anharmonicity Extends Carrier Lifetimes in Lead Halide Perovskites at Elevated Temperatures. *J. Phys. Chem. Lett.* **2019**, *10*, 6219−6226.

https://dx.doi.org/10.1021/acs.nanolett.0c04442
Nano Lett. 2021, 21, 756−761